

Progress in the growth and characterization of nonpolar ZnO films

Jin-Ju Chen · Xue-Ran Deng · Hong Deng

Received: 10 February 2012 / Accepted: 4 July 2012 / Published online: 18 July 2012
© Springer Science+Business Media, LLC 2012

Abstract Zinc oxide (ZnO) is an important material for its potential applicability to short-wavelength optoelectronic devices such as light emitting diodes (LEDs) and laser diodes (LDs). Nonpolar ZnO materials have been developed in recent years to avoid the strong internal electric fields in active regions of optoelectronic devices and improve luminescence efficiency. The growth and physical properties of nonpolar ZnO films, which are essential for fabricating optoelectronic devices and improving device performance, still remains not well understood. In this review, the technologies for preparation of nonpolar ZnO epitaxial films are summarized, and recent developments are described. Then the main characteristics of nonpolar ZnO films are discussed with the deviations from those of polar ZnO films, including morphology, structural defects, anisotropic strain, optical, and electrical properties. The anisotropic electron transport and strains correlated strongly with the anisotropic surface morphologies of nonpolar ZnO films. Fabricating nonpolar ZnO films with high quality should be further developed to decrease the structural defect densities for substantial improvement of device performance, and intensive studies on their characteristics are especially important for device applications.

Introduction

Zinc oxide (ZnO) is a direct band gap semiconductor material with a wide band gap of 3.37 eV at room

temperature, which enables its potential applications in short-wavelength optoelectronic devices such as blue or ultraviolet (UV)-light emitting diodes (LEDs) and laser diodes (LDs) [1–3]. In addition, ZnO is an excellent candidate for high efficiency laser operations because of the large exciton binding energy (60 meV). Since optically pumped lasing in epitaxially grown ZnO was observed at room temperature [4], ZnO has received more and more attention from researchers.

Most ZnO epitaxial films and their heterostructures such as (Zn, Mg)O/ZnO have been grown along the [0001] (*c*-axis) direction on foreign substrates. ZnO along the *c*-axis (polar ZnO) has alternate zinc ion layers with oxygen ion layers (as shown in Fig. 1a), which results in spontaneous polarization along the *c*-axis due to a lack of inversion symmetry. Piezoelectric polarization effect, as a result of the lattice-mismatch-induced strain in ZnO-based heteroepitaxial structures, also exists in ZnO crystal along the *c*-axis. Strong spontaneous and piezoelectric polarization effects lead to the build-in electric fields existing in the multi-quantum well devices [5, 6]. The magnitude of the internal electric field is as large as 0.9 MV/cm for the ZnO/Zn_{0.78}Mg_{0.22}O quantum wells [6]. Optical and electrical properties of devices are hampered by the internal electric field that separates the electron and hole wave functions in the quantum wells and consequently results in a decrease of internal quantum efficiency of the LEDs and LDs [7]. One approach to resolve this issue is to grow ZnO films without polarization field along the growth direction. ZnO {11 $\bar{2}$ 0} and {10 $\bar{1}$ 0} faces, in which there are equal numbers of zinc atoms and oxygen atoms, are parallel to the *c*-axis and considered as nonpolar *a*-plane and *m*-plane, respectively. The schematic atomic arrangements for nonpolar (11 $\bar{2}$ 0) plane and (1 $\bar{1}$ 00) plane are shown in Fig. 1b, c. Nonpolar

J.-J. Chen (✉) · X.-R. Deng · H. Deng
State Key Laboratory of Electronic Thin Films and Integrated
Devices, University of Electronic Science and Technology
of China, Chengdu 610054, People's Republic of China
e-mail: jinjuichen@uestc.edu.cn

ZnO is highly preferable for the optoelectronic devices because of the lack of spontaneous polarization field along the growth direction.

The polarity plays an important role in optical and electrical properties of ZnO films [8–10]. Therefore, investigations on the growth of nonpolar ZnO and their optical and electrical properties compared with that of polar ZnO are strongly motivated, and extensive research activities have been taken place all over the world in recent years. In this review, we first give a description of the growth of nonpolar ZnO films, and then outline the characteristics of nonpolar ZnO films, including surface morphologies, structural defects, strain, optical and electrical properties and so on. Finally, some concluding remarks and future research directions are put forward.

Growth of nonpolar ZnO films

We have summarized methods of nonpolar *a*-plane and *m*-plane ZnO films grown on different substrates in Table 1. Various techniques can be used to grow nonpolar ZnO

films, including metal organic chemical vapor deposition (MOCVD), molecular-beam epitaxy (MBE), pulsed laser deposition (PLD), radio frequency (RF) magnetron sputtering, and chemical vapor deposition (CVD), especially the first three techniques. The growth conditions, such as growth temperature [11–13, 31–34, 40–42, 48, 50–52, 69, 70], VI/II ratio [11, 12, 26, 46], oxygen pressure [12, 32, 72] and so on, have a significant influence on the crystalline quality and surface morphology of nonpolar ZnO films.

Various substrates, such as Al₂O₃, ZnO, LaAlO₃, LiTaO₃, LiAlO₂, and LiGaO₂, have been used to deposit nonpolar ZnO epitaxial films. Among them, *r*-plane and *m*-plane sapphires are the most common substrates for heteroepitaxial growth. The lattice periodicity of *r*-plane sapphire along [1 $\bar{1}$ 01] is 15.384 Å, which is almost three

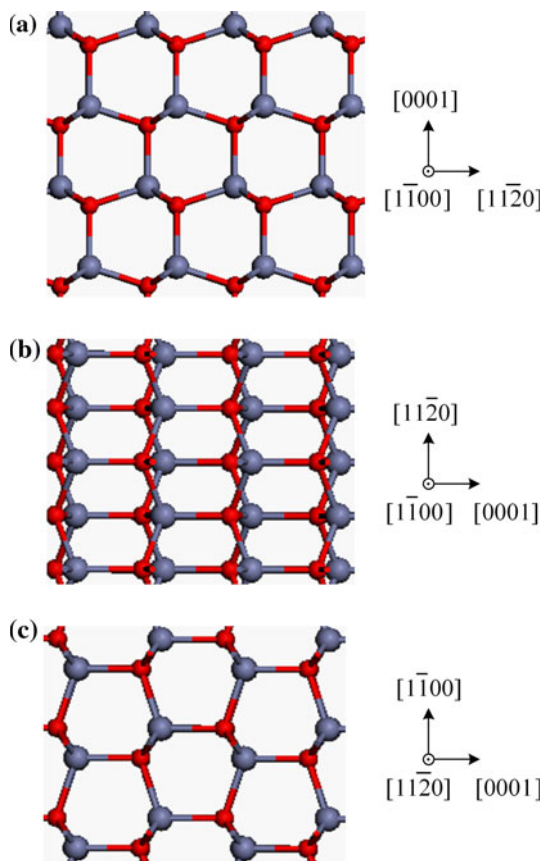


Fig. 1 Schematic atomic configurations of side views of the **a** *c*-plane, **b** *a*-plane, and **c** *m*-plane ZnO. Large and small spheres are Zn and O atoms, respectively

Table 1 Summary of ZnO films with different surfaces grown on different substrates

| Type | Surface orientation | Substrate type and orientation | Growth methods |
|------------------------------------|--|--------------------------------------|--|
| Nonpolar <i>a</i> -plane | (11 $\bar{2}$ 0) | (1 $\bar{1}$ 02) Sapphire | MOVPE [8–19] MBE [20–30] PLD [31–40] RF magnetron sputtering [41, 42] CVD [43, 44] |
| | | (11 $\bar{2}$ 0) ZnO | MOVPE [13, 45–47] |
| | | (100)LaAlO ₃ | MOVPE [48] PLD [49, 50] |
| | | (100) (La, Sr)(Al, Ta)O ₃ | CVD [51, 52] |
| | | (100) SrTiO ₃ | RF magnetron sputtering [53] |
| | | (302) γ -LiAlO ₂ | MOVPE [54] PLD [55] |
| | | (001) Si | PLD [56] |
| | | (01 $\bar{1}$ 2)LiTaO ₃ | MBE [57] |
| | | (010) LiGaO ₂ | RF magnetron sputtering [58] |
| | | Nonpolar <i>m</i> -plane | (10 $\bar{1}$ 0) |
| (10 $\bar{1}$ 0) ZnO | MBE [63–66] PLD [67, 68] | | |
| (100) LiGaO ₂ | RF magnetron sputtering [58] CVD [69, 70] | | |
| (100) γ -LiAlO ₂ | CVD [71, 72] MOCVD [73–75] | | |
| (001) MgO | MBE [76, 77] | | |
| (112)LaAlO ₃ | PLD [78–80] | | |

times of the lattice constant along ZnO[0001] (5.207 Å). The corresponding lattice mismatch along ZnO[0001] and $[\bar{1}100]$ is 1.54 and 18.3 %, respectively. ZnO (11 $\bar{2}0$) plane is parallel to Al₂O₃ (1 $\bar{1}02$) plane with an epitaxial relationship of $[\bar{1}100]\text{ZnO} \parallel [11\bar{2}0]\text{Al}_2\text{O}_3$ and $[0001]\text{ZnO} \parallel [1\bar{1}01]\text{Al}_2\text{O}_3$ for the nonpolar *a*-plane ZnO growth [15, 21, 24]. Compared with the pure *a*-plane ZnO films, which are easily grown on *r*-plane sapphire substrates, ZnO grains on *m*-plane sapphire substrates tend to grow parallel or perpendicular to the *c*-axis direction depending on the growth conditions. Moriyama and Fujita reported *m*-plane ZnO grown on *m*-plane sapphire substrates [11]. They found both higher growth temperature (800 °C) and higher VI/II ratio (2.8×10^4) were needed in the growth of pure *m*-plane ZnO, and the epitaxial relationship was found to be $[0001]\text{ZnO} \parallel [2\bar{1}\bar{1}0]\text{Al}_2\text{O}_3$ and $[\bar{2}110]\text{ZnO} \parallel [0001]\text{Al}_2\text{O}_3$, while lower growth temperature (500 °C) or lower VI/II ratio (5.4×10^3) resulted in the formation of (01 $\bar{1}3$) planes in addition to (01 $\bar{1}0$) planes. The *m*-plane ZnO films were not found to be pure and (10 $\bar{1}3$) domains initiated inside the film were also observed above the ZnO/Al₂O₃ interface in other researches [61, 62]. For *m*-plane sapphire, the lattice constant along the *c*-axis [0001] Al₂O₃ is 12.990 Å, which is almost four times of the lattice constant along the $[\bar{2}110]$ ZnO (3.250 Å), with a mismatch of only 0.077 %, while the lattice misfit along the $[\bar{2}\bar{1}\bar{1}0]\text{Al}_2\text{O}_3$ and [0001] ZnO is 9.66 %. In epitaxial growth, lattice mismatch between an epilayer and a substrate plays a crucial role. Due to the high lattice mismatch, *r*-plane and *m*-plane sapphire substrates usually reduce the crystalline quality of nonpolar ZnO films significantly, and the nonpolar ZnO films with high quality have not been obtained so far [9, 27, 44, 73]. One solution to mitigate the large lattice mismatch between ZnO and sapphire is to use GaN or SiN_x as the buffer layer on sapphire substrates [37, 39, 42], and results demonstrate that *a*-plane ZnO films with high crystallinity have been successfully obtained.

Other suitable substrates that exhibit smaller lattice mismatch with ZnO have been chosen as shown in Table 1. In particular, the homoepitaxial growth without any lattice mismatch has attracted attention to achieve nonpolar ZnO films with smooth surfaces and low density of intrinsic defects. Kashiwaba et al. [13] made a comparative study on *a*-plane ZnO films deposited on single crystal ZnO (11 $\bar{2}0$) and sapphire (1 $\bar{1}02$) substrates. The full-width at half-maximum (FWHM) of rocking curve for (0002) plane of homoepitaxial ZnO film was smaller by one order of magnitude than that of heteroepitaxial ZnO film in grazing incident diffraction (GID) measurement. Meanwhile, the optical property of homoepitaxial ZnO film was better than that of heteroepitaxial ZnO film. Abe et al. [47] used ZnO (11 $\bar{2}0$) substrates with off-angles to obtain *a*-plane ZnO

epitaxial films, and they found that the surface morphology and crystal quality of films were remarkably improved. These researches indicate that single crystal ZnO (11 $\bar{2}0$) substrates are advantageous for the growth of high-quality *a*-plane ZnO films. Homoepitaxial growth of nonpolar *m*-plane ZnO was intensively investigated by laser-MBE [63–66]. Nanostripe arrays along the [0001] direction could be naturally formed on ZnO (10 $\bar{1}0$) surface and the lateral periodicity of arrays could be controlled by growth conditions.

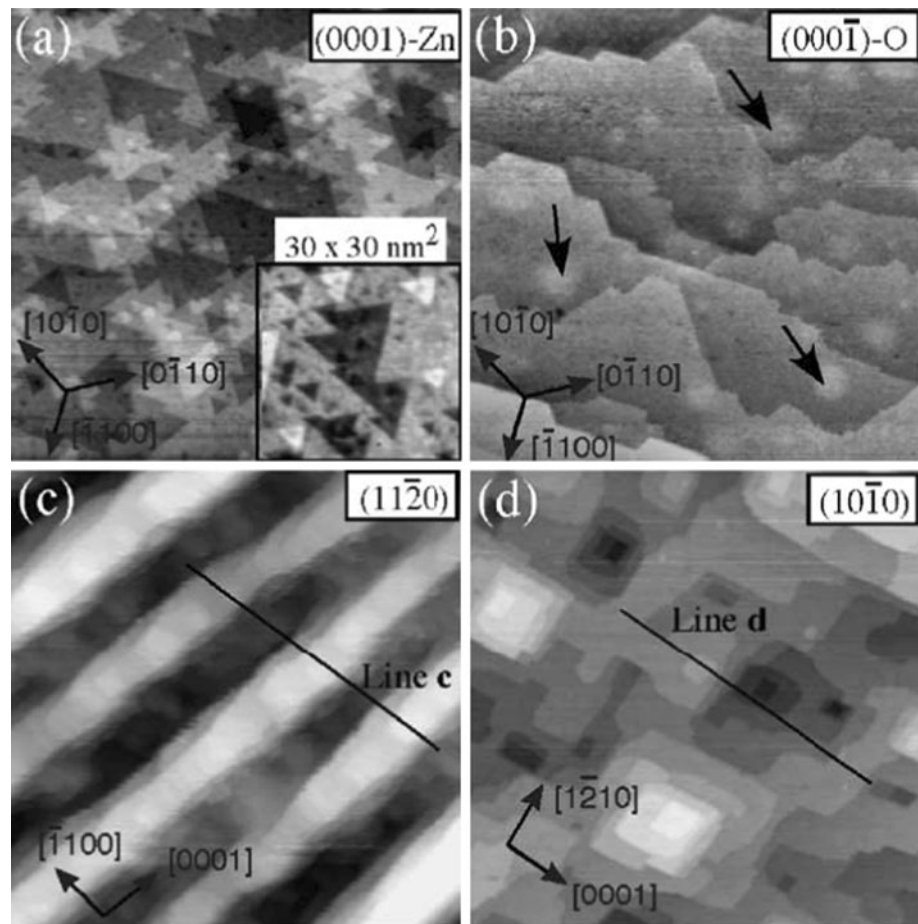
Properties of nonpolar ZnO films

Morphology

The surface of nonpolar film is expected to be smooth in a specific direction and there is an anisotropic character in surface morphology. A smooth surface could be obtained under the condition in which the lateral growth along the *c*-axis direction is greatly enhanced. Atomic-scale properties of low-index ZnO surfaces have been characterized with high-resolution scanning tunneling microscopy (STM) (Fig. 2) [81]. The surface morphologies for (11 $\bar{2}0$) and (10 $\bar{1}0$) ZnO films are obviously different from those of polar ZnO. Deep grooves with steep, [0001]-oriented sides are regularly spaced on (11 $\bar{2}0$) surface from Fig. 2c. Nanoscale striped pattern along the ZnO[0001] direction was also observed on (11 $\bar{2}0$) ZnO films in other researches [13, 21, 39, 45–47]. The average width of the stripes varies with the preparation conditions. The origin of stripes parallel to the ZnO[0001] direction is possibly related to a large anisotropy of the lattice misfits in orthogonal direction [21]. The small lattice mismatch along the ZnO *c*-axis direction might enhance the lateral growth characteristics. ZnO (10 $\bar{1}0$) surface has been revealed rectangular terraces with step edges running along the [0001] and the $[\bar{1}210]$ direction as shown in Fig. 2d. The well-defined terrace-step structure can be influenced by the preparation parameters and the sample miscut [71, 82].

Nanoscale determination of surface orientation of nonpolar ZnO films was intensively investigated by Zúñiga-Pérez et al. [16, 17, 60]. Some developed facets inclined to the nonpolar ZnO surface were observed, and the orientation of surface facets was determined by scanning force microscopy (SFM) technique. The surface of *a*-plane ZnO film grown on *r*-plane sapphire by metal–organic vapor phase epitaxy (MOVPE) consists of rhombohedral pyramids, whose longest axis is parallel to the [0001] direction and sidewalls are shown to be $\{10\bar{1}1\}$ -type planes (Fig. 3) [16]. Faceted surface of nonpolar (11 $\bar{2}0$) ZnO was also observed by RHEED pattern [21]. Similar growth feature

Fig. 2 Scanning tunneling microscopy (STM) results (a–d) of ZnO surfaces after sputtering and annealing in ultrahigh vacuum. All images are 200×200 nm in size and were taken with tunneling parameters $V_{\text{Bias}} = +2$ V and $I_{\text{tunnel}} = 1.5$ nA. All surfaces show a (1×1) termination in LEED. **a** The Zn terminated (0001) -Zn surface is characterized by many triangular islands with monatomic step height. Step edges are O-terminated, and the resulting non-stoichiometry stabilizes this polar surface. **b** The O-terminated $(000\bar{1})$ surface exhibits stoichiometric double-steps with a 120° angle. The bright spots marked with arrows are attributed to subsurface impurities. **c** The $(11\bar{2}0)$ surface exhibits deep and regular ridges. **d** The $(10\bar{1}0)$ surface has a regular terrace-step structure with rectangular islands. Reprinted from [81] with permission from Elsevier

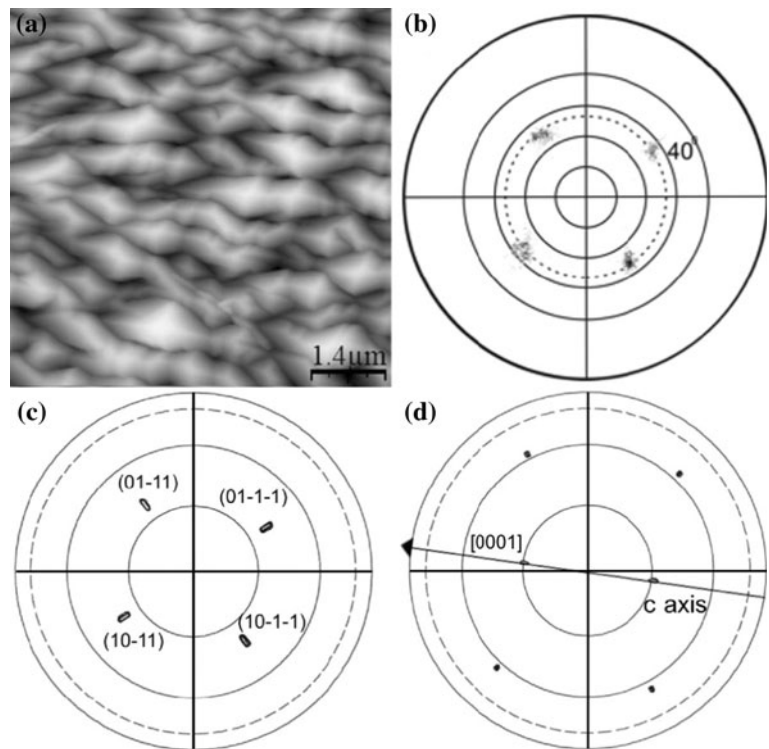


has been seen from $(10\bar{1}0)$ ZnO film grown on *m*-plane sapphire by MOVPE [60]. With the film thickness increasing, the grains were elongated along the $[0001]$ direction and developed well-defined crystallographic facets. The formation of $\{30\bar{3}2\}$ - and $\{30\bar{3}\bar{2}\}$ -type facets first occurred, then $\{30\bar{3}2\}$ - and $\{30\bar{3}\bar{2}\}$ -type facets with $\{10\bar{1}1\}$ - and $\{10\bar{1}\bar{1}\}$ -type facets coexisted, and finally, the surface was covered by $\{10\bar{1}1\}$ - and $\{10\bar{1}\bar{1}\}$ -type facets, although some $\{30\bar{3}2\}$ - and $\{30\bar{3}\bar{2}\}$ -type facets remained. The origin of this faceting was discussed in terms of thermodynamic stability and kinetics arguments [60]. However, for ZnO $(10\bar{1}0)$ homoepitaxial film formed using laser-MBE, self-organized nanostripe arrays running along the $[0001]$ direction were observed on film surface, and the nanostripe arrays were triangular-shaped in cross section and two side bonding facets were composed of high-index $(31\bar{4}0)$ and $(4\bar{1}\bar{3}0)$ planes [63–65], which were explained in terms of a step-faceting mechanism based on Schwoebel barrier and nonthermal equilibrium growth. Researchers all consider that the surface energy needed for the formation of facets is lower than that required for ZnO $(11\bar{2}0)$ or $(10\bar{1}0)$ surface despite the differences in their studies [16, 60, 63]. The surface electrical properties of nonpolar ZnO

films are dramatically affected by these highly anisotropic surfaces.

Investigations on the growth of ZnO films with different orientations suggest that the surface roughness of epitaxial films grown along the $[0001]$ direction have always been found to be superior to that of nonpolar films [9, 66]. Nonpolar orientations display a large surface roughness due to the formation of well-developed facets [16, 60, 63]. Diebold et al. [81] also showed that the nonpolar *a*-plane of bulk ZnO crystals with anisotropic features oriented parallel to the crystallographic *c*-axis, was rougher than the polar *c*-plane, while $(10\bar{1}0)$ surface exhibited less roughness compared with $(11\bar{2}0)$ surface. The rough surface of nonpolar ZnO films makes it difficult to be used for device fabrication. Interface roughness will affect the mobility of two-dimensional electrons, and interface roughness scattering is the dominant scattering mechanism in thin quantum wells [83]. A slight roughness in the heterointerfaces results in a large fluctuation in quantization energy of confined electrons [67]. It is imperative to study and control the surface morphology of nonpolar ZnO films for developing heterostructure devices.

Fig. 3 **a** Topography image of the ZnO surface consists of rhombohedral-base pyramids. **b** Calculated topographic normals distribution show that the facets form $40^\circ \pm 2^\circ$ with respect to the growth direction. **c** Experimental pole figure of ZnO $\{10\bar{1}1\}$ reflections confirms the $\{10\bar{1}1\}$ -type planes covered the ZnO surface. **d** Pole figure of ZnO $\{11\bar{2}1\}$ reflections. The polar $[0001]$ axis is seen to be parallel to the pyramids longest axis, indicating that the stripes in ZnO surface are aligned along the $[0001]$ axis. (Reprinted figure with permission from [16]. Copyright (2005) by the American Physical Society.)



Microstructure and defects

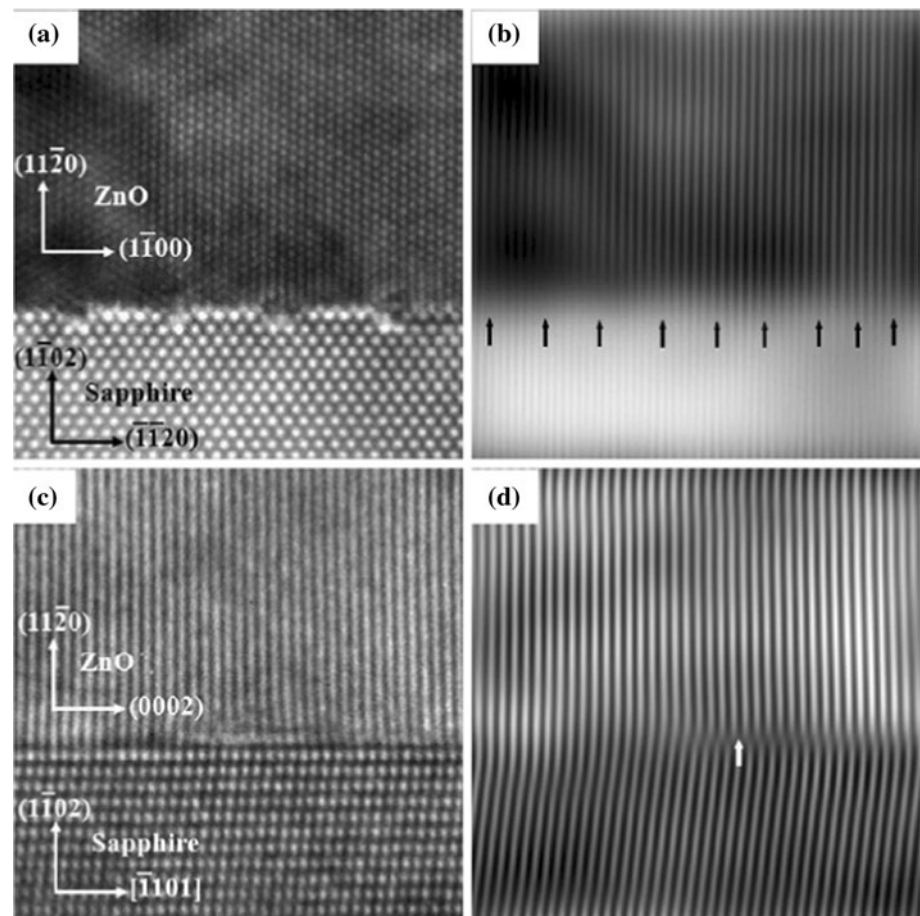
The structural defects have a direct influence on the optical and electrical properties of films and devices. One of the decisive issues for the realization of high-quality nonpolar GaN films is the high density of stacking faults (SFs) in addition to the high-density threading dislocations (TDs). As a fundamental competitor for GaN, there are also high density of defects such as SFs and dislocations in nonpolar ZnO [20, 23, 24]. High-resolution TEM (HRTEM) studies are usually performed to investigate the interfaces and dislocations in films. Defects in *a*-plane ZnO films on *r*-plane sapphire substrates are revealed to be misfit dislocations (MDs) at the interface [84], basal SFs, and TDs or partial dislocations (PDs) in the films [23, 24]. The interfaces between ZnO (11 $\bar{2}$ 0) films and Al₂O₃ (1 $\bar{1}$ 02) substrates are atomically sharp and semicoherent, which can be observed from TEM micrographs in Fig. 4 [23]. This sharp interface property is required for the growth of high-quality heterostructures and quantum wells. Zone axes of Fig. 4a, c are ZnO $\langle 0001 \rangle$ and ZnO $\langle \bar{1}100 \rangle$, respectively. The MDs are clearly visible as marked by arrows at the interface with regularly spaced configurations in Fig. 4b. However, the MDs are rarely observed due to the small lattice misfit (1.54 %) along the ZnO $\langle 0001 \rangle$ direction in Fig. 4d.

In addition to MDs at the *a*-ZnO/*r*-sapphire interfaces, SFs and TDs are observed in the films. TDs are observed without the appearance of SFs with $g = 0002_{\text{ZnO}}$ in

Fig. 5a, and most SFs and a few TDs are observed with $g = 1\bar{1}00_{\text{ZnO}}$ in Fig. 5b [23]. Dislocation densities are estimated to be $\sim 7.3 \times 10^{10} \text{ cm}^{-2}$ for the dislocations with $\langle 0001 \rangle$ Burgers vector in Fig. 5a and $\sim 6.1 \times 10^9 \text{ cm}^{-2}$ for the dislocations with $1/3\langle 11\bar{2}0 \rangle$ Burgers vector in Fig. 5b. The SF in Fig. 5b is the type-I₁ intrinsic stacking fault with a displacement vector of $1/6\langle 02\bar{2}3 \rangle$ having the Frank partial dislocations at the end of the SF. And the SF density is estimated to be $\sim 1.2 \times 10^5 \text{ cm}^{-1}$ [23]. Similar type-I₁ intrinsic stacking faults have been observed in other *a*-plane ZnO films grown on *r*-plane sapphire substrates [24] or on *r*-plane LiTaO₃ substrates [57], and the SF density is almost at the same magnitude [24]. Lee et al. [23] found the strain relaxation in films was dominantly accommodated by the diagonal defects in the thinner film but it was accommodated mainly by the TDs in the thicker film in addition to the MDs. Interestingly, the TDs are being the perfect dislocations not the PDs in Lees' research, while Vennéguès et al. [24] think that the microstructure of *a*-plane ZnO films is dominated by SFs and related PDs with density of $(4\text{--}7) \times 10^{10} \text{ cm}^{-2}$.

For nonpolar *m*-plane ZnO films grown on *m*-plane sapphire substrates, MDs distributed at the ZnO/Al₂O₃ interfaces and were orientation-dependent and quite anisotropic. Meanwhile, type-II SFs bounded by the Frank dislocations with the Burgers vector of $1/6\langle 20\bar{2}3 \rangle$ were also observed at the interface [62]. Similar defects in *m*-plane ZnO films epitaxially grown on (112) LaAlO₃ substrate

Fig. 4 HRTEM micrographs at the interfaces between *a*-plane ZnO films and *r*-plane sapphire substrates. **a** ZnO[0001] zone axis HRTEM micrograph, **b** Fourier-filtered image corresponding to the image in (a), **c** ZnO[$\bar{1}100$] zone axis HRTEM micrograph, and **d** Fourier-filtered image corresponding to the image in (c). Misfit dislocations at the interfaces are marked by arrows. Reprinted from [23] with permission from Elsevier



were observed, and the densities of dislocations and SFs were estimated to be $5.1 \times 10^{10} \text{ cm}^{-2}$ and $4.3 \times 10^5 \text{ cm}^{-1}$, respectively [80].

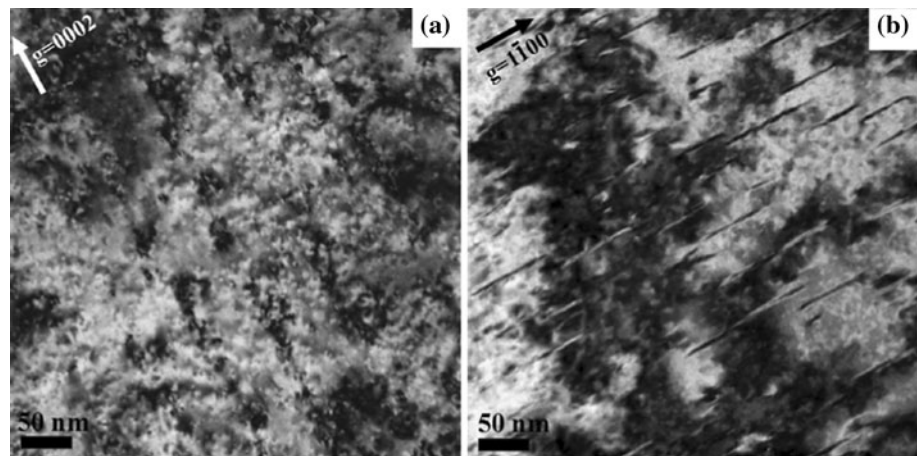
Basal SFs and TDs have a significant impact on the optical and electrical properties of ZnO, and have been a major obstacle to the development of nonpolar ZnO. However, there are still very few reports on how to reduce extended defect densities in films, and extensive study on that is expected. In our humble opinions, there are some possible ways to decrease the SF and dislocation densities: further optimization or new approaches need to be used to fabricate films with low defect density for heteroepitaxial growth; in addition, various nucleation layers, such as low temperature ZnO and high temperature ZnO, or buffer layer could be used to enhance the lateral growth and improve the crystallinity; and high-quality nonpolar ZnO bulk substrates for homoepitaxial growth of nonpolar ZnO films with low defect density should be further developed.

Strain

Considerable residual strains can be induced in ZnO films grown on sapphire substrates by lattice and thermal

expansion mismatches. The in-plane strain in nonpolar layers is strongly anisotropic due to anisotropic in-plane lattice mismatch [14, 29, 35], which breaks the crystal symmetry from wurtzite C_{6v} to orthorhombic C_{2v} , and strongly influences the valence band structure and related selection rule [28, 35, 85]. The nonpolar $[1\bar{1}00]$ direction is under tensile strain and polar $[0001]$ direction is under compressive strain, and in-plane strain anisotropy increases with increasing of film thickness due to faster relaxation along $[1\bar{1}00]$ direction [14]. Anisotropic in-plane biaxial strain leads to a distortion of the hexagonal symmetry of the ZnO basal plane [36]. Strain relaxation is also strongly anisotropic along the two perpendicular in-plane directions of $[1\bar{1}00]$ ZnO and $[0001]$ ZnO [27, 36, 37]. For the large lattice mismatch $[1\bar{1}00]$ ZnO direction, the misfit strain can be fully relaxed by the generation of geometrical misfit dislocations due to activation of low energy prismatic slip systems, while for the small misfit $[0001]$ ZnO direction, the strain is only partially relaxed by dislocation nucleation at the free surface due to a lack of activated systems [27, 36]. It was observed that the complete anisotropic strain relaxation required the film thickness to be larger than $\sim 800 \text{ nm}$ [86], and even larger than $2 \mu\text{m}$ [14].

Fig. 5 Plan-view TEM micrographs of the 240 nm-thick *a*-plane ZnO film. **a** $g = 0002_{\text{ZnO}}$ and **b** $g = 1\bar{1}00_{\text{ZnO}}$ two-beam BF micrographs. Perfect threading dislocations with a Burgers vector of $\langle 0001 \rangle$ were dominantly observed in **(a)**, while the stacking faults were mainly observed in **(b)**. Reprinted from [23] with permission from Elsevier



Anisotropic strain and strain relaxation will significantly affect the properties of nonpolar ZnO-based devices.

Raman spectra can be performed to estimate residual stress in ZnO films through the frequency shifts of E_2 high mode relative to the single crystal value [35, 40, 75]. Compressive stress existed in *a*-plane and *m*-plane ZnO films grown on LiGaO₂ (010) and (100), respectively [58]. Compressive stress was also observed in *a*-plane ZnO films on (302) γ -LiAlO₂ substrates [54, 55], while *m*-plane ZnO film grown on (100) γ -LiAlO₂ was under a slight tensile stress [75]. Anisotropic mismatch and strain pose a challenge toward the growth of nonpolar ZnO films and their heterostructures, especially the control of surface and interface.

Optical properties

The optical properties of nonpolar ZnO films have been intensively studied by photoluminescence (PL) and photorefectivity (PR) spectra. Two different features in optical properties of nonpolar ZnO films can be seen from that of polar ZnO films. The first difference is related to the anisotropic in-plane character of the optical properties, which is manifested by a strong polarization. The second difference is related to their lower crystalline qualities and is characterized by additional emission bands attributed to structural defects such as SFs.

Anisotropic strain and the orientation of nonpolar plane play important roles in determining the polarization selectivity and properties of excitonic transitions [87]. Nonpolar (11 $\bar{2}$ 0) ZnO films displayed polarization-dependent excitonic resonance structures according to the polarization selection rules for anisotropically strained ZnO [21, 28, 87]. There was only a strong E_1 at lower energies for $E \perp c$, and both E_1 and E_2 are observed for $E \parallel c$ in thin (100 nm) *a*-plane ZnO, whereas E_1 is significantly weaker than E_2 [87] (Fig. 6). However, a single resonant

feature was observed for $E \parallel c$ in strained thick ($\sim 1 \mu\text{m}$) *a*-plane ZnO [28]. In-plane optical anisotropy under different polarization conditions was also evident from polarized transmission spectra [19, 74] and Raman spectra [54, 74]. This pronounced polarization-dependent emission in nonpolar ZnO films suggests a potential usage as polarization-sensitive optoelectronic devices.

The crystalline quality of *a*-plane ZnO films on *r*-plane sapphire substrates is generally inferior compared with that of polar ZnO films synthesized on *a*-plane or *c*-plane sapphire substrates, which results in weaker intensity of UV emission from nonpolar ZnO than that from polar ZnO [9, 10]. Moreover, strong residual anisotropic strains in *a*-plane ZnO films grown on *r*-plane sapphire can cause significant blueshift of the transition energies compared with those in strain-free polar ZnO films [28]. Furthermore, the feature of near-band-edge (NBE) emission in nonpolar ZnO film is similar to the characteristic of UV emission shown in many *p*-type doped ZnO materials, i.e., acceptor-related emissions were observed in *a*-plane or *m*-plane ZnO films [37, 56, 64, 77], which were explained by localized-acceptor states induced by basal plane SFs. Two lower-energy features at 3.386 and 3.326 eV were observed in PR spectra (Fig. 6), which were assigned to be neutral donor-bound exciton emission (DX) and free-electron-to bound transition ($e-A_0$), respectively [87]. The DX line is an E_1 exciton bound to a donor. The exciton localization energy to the donor (34 meV) in nonpolar ZnO is much larger than that (~ 16 meV) in polar ZnO. This is consistent with what has been reported in the literature [37]. The temperature-dependent PL spectra of *a*-plane ZnO shown in Fig. 7b does not show any signature of free excitons up until room temperature [87]. This result indicates that the DX emission will dominate the emission from highly strained *a*-plane ZnO even at room temperature, and this also supports the fact that the localization energy of the DX in nonpolar ZnO is much larger than that in polar ZnO.

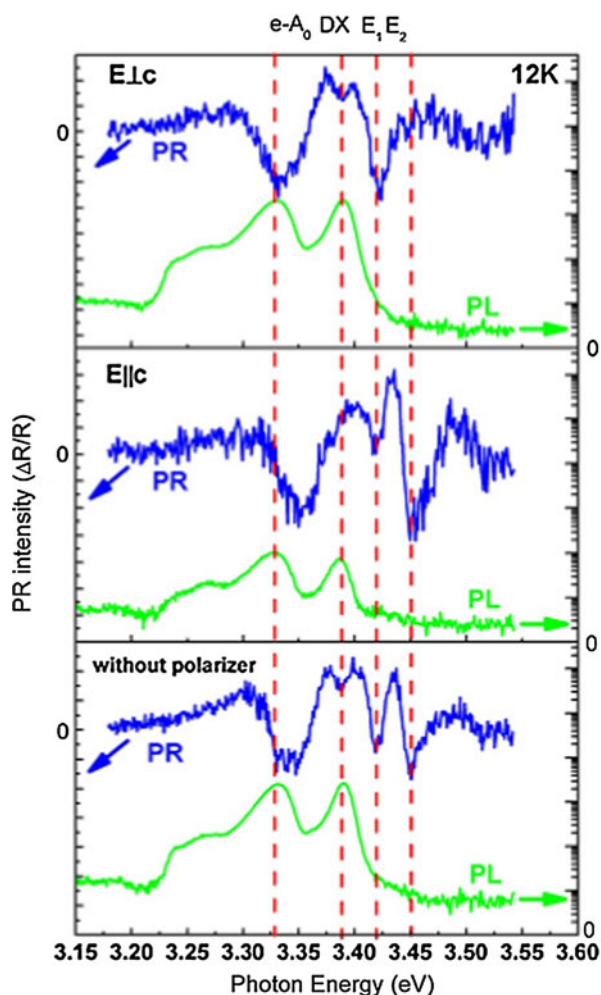


Fig. 6 Polarization-dependent PR and PL spectra at 12 K. The top and middle panels represent $E \perp c$ and $E \parallel c$ polarizations, respectively. The bottom panel shows the spectra without the polarizer. Reprinted with permission from [87]. Copyright 2008, American Institute of Physics

Unlike the highly strained *a*-plane ZnO, temperature-dependent PL spectra of *m*-plane ZnO under a small tensile stress show a free exciton emission with the temperature lower than 138 K [75]. The $e-A_0$ transition related to acceptor defects has also been observed by several authors in nonpolar ZnO [37, 56, 77]. In addition, a violet-blue emission ascribed to the electron transitions from the conduction band to V_{Zn} defect state was observed in literatures [9, 37, 56], which was not present in *c*-plane ZnO film [9]. Diebold demonstrated the presence of point defect V_{Zn} in *a*-plane ZnO by high-resolution scanning tunneling microscopy [81]. V_{Zn} was identified as the dominant defect in *a*-plane ZnO, and the V_{Zn} concentration was detected to be $\sim 2 \times 10^{17} \text{ cm}^{-3}$ by positron annihilation spectroscopy [18]. In nonpolar *m*-plane ZnO film, V_{Zn} related defects were also verified by positron annihilation spectroscopy [59].

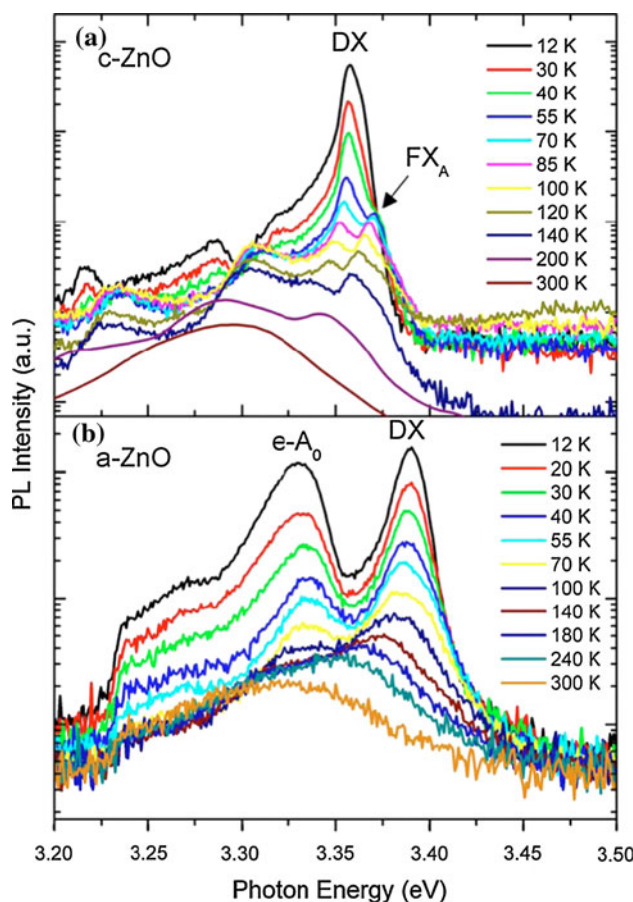


Fig. 7 Temperature-dependent PL spectra of polar **a** and nonpolar **b** ZnO films Reprinted with permission from [87]. Copyright 2008, American Institute of Physics

Electrical properties

Polar ZnO and nonpolar ZnO have large difference in the electron mobility. It is well known that the mobility is strongly dependent on defect concentration and scattering mechanism. The defect concentration in nonpolar ZnO is higher than that in polar ZnO, which is responsible for low electron mobility, and the anisotropic distribution of SFs in nonpolar ZnO will also attribute to the large electron mobility difference between nonpolar ZnO and polar ZnO.

Nonpolar planes are expected to yield large in-plane anisotropy in electrical characteristic. Matsui et al. [63–65] reported homoepitaxial growth of nonpolar *m*-plane ZnO with dense arrays of one-dimensional nanostructures. This highly anisotropic surface morphology resulted in electron transport of nonpolar ZnO layers and $\text{Mg}_{0.12}\text{Zn}_{0.88}\text{O}/\text{ZnO}$ multi-quantum wells (MQWs) with conductivity parallel to the nanostructure arrays being more than one order of magnitude larger than that perpendicular to the nanostructure arrays.

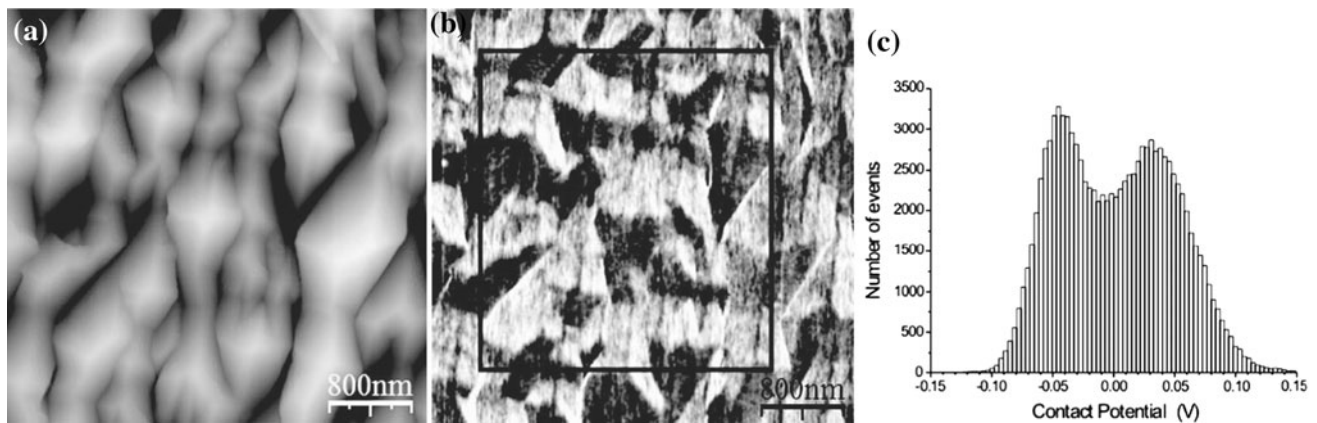


Fig. 8 **a** Topography and **b** surface contact potential images of ZnO (1120) surface. Topographic and contact potential images are of the same surface area. **c** Contact potential distribution measured inside

the solid square shown in **(b)**. (Reprinted figure with permission from [16]. Copyright (2005) by the American Physical Society.)

The origin of anisotropic conductivity was mainly from anisotropically distributed scattering centers of electrons related to grain boundaries between nanostripe arrays.

The development of polar facets leads to electrically inhomogeneous surfaces (Fig. 8) [16, 17, 60]. ZnO (1120) surface was covered by $\{10\bar{1}1\}$ and $\{10\bar{1}\bar{1}\}$ planes in Fig. 8a. Bright and dark contrast regions in Fig. 8b were due to the charge density variations, which indicated different charge domains alternated along the [0001] direction. One can see a clear correlation between morphological facets and contact potential from the comparison of Fig. 8a, b. There were two types of charge domains existing in film surface seen from Fig. 8c. Facets in nonpolar ZnO films tend to expose polar regions with different work functions that affect electron transport properties across the surface. Meanwhile, polar regions accompanied by electrostatics fields will decrease device efficiency. So faceting into polar surfaces must be prevented by controlling preparation parameters to obtain heterostructures free of electrostatic fields.

p-Type doping and quantum wells structure

Few studies on realizing *p*-type conduction in nonpolar ZnO have been reported. Research by Gangil et al. [8] showed that nitrogen doping as the acceptor mode existed in nonpolar (1120) ZnO films with less donor complexes; that was, nonpolar crystal orientation had a positive effect on the chemical bonding states of nitrogen-doped ZnO for attaining *p*-type conductivity. The nonintentionally doped nonpolar *m*-plane ZnO layers exhibited a residual doping as low as $\sim 10^{14} \text{ cm}^{-3}$ [88], which is one order of magnitude lower than that in polar (0001) ZnO [89]. Tainoff et al. [88] thinks that the nonpolar orientation is of benefit

to reach *p*-type ZnO films because of such low residual doping. However, *p*-type doping is still not achieved by nitrogen doping despite of effective acceptor incorporation due to strong compensation in *m*-plane ZnO:N films. Other research showed that the nonintentionally doped *m*-plane ZnO film grown under oxygen-rich condition exhibited weak *p*-type conductivity with a hole concentration of $1.3 \times 10^{16} \text{ cm}^{-3}$ [90]. Dai et al. [91] prepared intrinsic *p*-type ZnO film with (10 $\bar{1}$ 0) preferred orientation by single source chemical vapor deposition (SSCVD). *p*-Type conductivity of this film was more stable than that of ZnO film with *c*-axis orientation after nitrogen doping [92].

As predicted by theory, there is no built-in electric field and less carrier localization effects existing in *a*-plane ZnO/ZnMgO MQWs [93]. Chauveau et al. [20, 22, 29, 94–96] intensively studied *a*-plane (1120) ZnO quantum wells (QWs) from the growth of ZnO/(Zn, Mg)O quantum well structures to their properties. There exhibits confinement effect but no quantum-confined Stark effect in nonpolar ZnO/(Zn, Mg)O QWs, contrary to that in *c*-oriented structures. Similar phenomenon has been observed in homoepitaxial ZnO/(Zn, Mg)O quantum well grown on *m*-plane oriented substrate [97]. $\text{Mg}_{0.12}\text{Zn}_{0.88}\text{O}/\text{ZnO}$ QWs revealed strong in-plane anisotropy in electrical and optical characteristics due to highly anisotropic surface morphologies and anisotropic strains [65–68]. Anisotropy strain in QWs induced a strong blueshift of excitonic transitions [29, 94]. Homoepitaxial nonpolar QWs are more conducive to strong UV emission because of the reduction of structural defects and the improvement of surface morphology [94, 95]. Heteroepitaxial nonpolar QWs with high crystalline quality on substrate involving a large lattice misfit may be obtained through new paradigms such as domain-matching epitaxy reported by Narayan [98].

Summary

Nonpolar ZnO has potential applications in short-wavelength optoelectronic devices due to overcoming the negative effects of strong internal electric fields. There are strong research efforts to investigate and develop high-quality nonpolar ZnO films. However, most results are not promising for device applications because of low crystal quality, high defects density, and large surface roughness. The intensive growth optimizations, including various growth methods, precise control of parameters, homoepitaxial growth or using the buffer layer on foreign substrates, have been made to improve the crystalline quality, reduce the defect density and decrease the surface roughness. But it is thought that further improvements in crystalline quality and surface roughness are still required for practical application.

At the present time, several other issues, such as *p*-type doping and QWs structures are still not clear and remain to be clarified. The detailed studies and thorough understanding of the specific properties of nonpolar ZnO are also of critical importance toward device applications. The application of nonpolar ZnO material for optoelectronic devices remains under development, which should be exploited progressively. In short, a lot of detailed work is indeed necessary and should be done before ZnO films with nonpolar surfaces can be applied in optoelectronic devices.

Acknowledgements The authors wish to thank the Chinese Nature Science Fundamental Committee (Grant No.: 50802012) for financial support.

References

- Jiao SJ, Zhang ZZ, Lu YM, Shen DZ, Yao B, Zhang JY, Li BH, Zhao DX, Fan XW, Tang ZK (2006) *Appl Phys Lett* 88:031911
- Ryu Y, Lee TS, Lubguban JA, White HW, Kim BJ, Park YS, Youn CJ (2006) *Appl Phys Lett* 88:241108
- Aoki T, Hatanaka Y, Look DC (2000) *Appl Phys Lett* 76:3257
- Bagnall DM, Chen YF, Zhu Z, Yao T, Koyama S, Shen MY, Goto T (1997) *Appl Phys Lett* 70:2230
- Makino T, Ohtomo A, Chia CH, Segawa Y, Koinuma H, Kawasaki M (2004) *Physica E* 21:671
- Morhain C, Bretagnon T, Lefebvre P, Tang X, Valvin P, Guillet T, Gil B, Taliercio T, Teisseire-Doninelli M, Vinter B, Deparis C (2005) *Phys Rev B* 72:241305(R)
- Wetzel C, Takeuchi T, Amano H, Akasaki I (2000) *Phys Rev B* 62:R13302
- Gangil S, Nakamura A, Shimomura M, Temmyo J (2007) *Jpn J Appl Phys* 46:L549
- Zhu JJ, Aaltonen T, Venkatachalapathy V, Galeckas A, Yu Kuznetsov A (2008) *J Cryst Growth* 310:5020
- Zhang Y, Du G, Zhu H, Hou C, Huang K, Yang S (2004) *Opt Mater* 27:399
- Moriyama T, Fujita S (2005) *Jpn J Appl Phys* 44:7919
- Chen HG, Chen GJ, Jian SR, Huang GZ, Ni JW (2009) *Int J Mod Phys B* 23:1154
- Kashiwaba Y, Abe T, Onodera S, Masuoka F, Nakagawa A, Endo H, Niikura I, Kashiwaba Y (2007) *J Cryst Growth* 298:477
- Saraf G, Lu Y, Siegrist T (2008) *Appl Phys Lett* 93:041903
- Gorla CR, Emanetoglu NW, Liang S, Mayo WE, Lu Y, Wraback M, Shen H (1999) *J Appl Phys* 85:2595
- Zúñiga-Pérez J, Muñoz-Sanjosé V, Palacios-Lidón E, Colchero J (2005) *Phys Rev Lett* 95:226105
- Zúñiga-Pérez J, Palacios-Lidón E, Muñoz-Sanjosé V, Colchero J (2007) *Appl Phys A* 88:77
- Zubiaga A, Tuomisto F, Zúñiga-Pérez J, Muñoz-Sanjosé V (2008) *Acta Phys Pol A* 114:1457
- Saraf G, Zhong J, Dulub O, Diebold U, Siegrist T, Lu Y (2007) *J Electron Mater* 36:446
- Chauveau JM, Laugt M, Vennegues P, Teisseire M, Lo B, Deparis C, Morhain C, Vinter B (2008) *Semicond Sci Technol* 23:035005
- Han SK, Hong SK, Lee JW, Lee JY, Song JH, Nam YS, Chang SK, Minegishi T, Yao T (2007) *J Cryst Growth* 309:121
- Chauveau J-M, Buell DA, Laiigt M, Vennégues P, Teisseire-Doninelli M, Berard-Bergery S, Deparis C, Lo B, Vinter B, Morhain C (2007) *J Cryst Growth* 301–302:366
- Lee JW, Han SK, Hong S-K, Lee JY, Yao T (2008) *J Cryst Growth* 310:4102
- Vennégues P, Chauveau JM, Korytov M, Deparis C, Zuniga-Perez J, Morhain C (2008) *J Appl Phys* 103:083525
- Lee JW, Han SK, Hong S-K, Lee JY (2010) *Appl Surf Sci* 256:1849
- Han SK, Kim J-H, Hong S-K, Song J-H, Song J-H, Lee JW, Lee JY, Hong SI, Yao T (2010) *J Cryst Growth* 312:2196
- Chauveau J-M, Vennégues P, Laiigt M, Deparis C, Zuniga-Perez J, Morhain C (2008) *J Appl Phys* 104:073535
- Koida T, Chichibu SF, Uedono A, Sota T, Tsukazaki A, Kawasaki M (2004) *Appl Phys Lett* 84:1079
- Chauveau J-M, Vives J, Zuniga-Perez J, Laiigt M, Teisseire M, Deparis C, Morhain C, Vinter B (2008) *Appl Phys Lett* 93:231911
- Vennegues P, Zhu T, Bougrioua Z, Martin D, Zuniga-Perez J, Grandjean N (2009) *Jpn J Appl Phys* 48:090211
- Han SK, Hong S-K, Lee JW, Kim JG, Jeong M, Lee JY, Hong SI, Park JS, Ihm YE, Ha J-S, Yao T (2011) *Thin Solid Film* 519:6394
- Song H, Kim J-H, Kim EK (2009) *J Korean Phys Soc* 55:1098
- Elanchezhian J, Bae KR, Lee WJ, Shin BC, Kim SC (2010) *Mater Lett* 64:1190
- Pant P, Budai JD, Aggarwal R, Narayan Roger J, Narayan J (2009) *Acta Mater* 57:4426
- Kuo CC, Liu W-R, Hsieh WF, Hsu C-H, Hsu HC, Chen LC (2009) *Appl Phys Lett* 95:011905
- Pant P, Budai JD, Narayan J (2010) *Acta Mater* 58:1097
- Han X, Gao Y, Dai J, Yu C, Wu Z, Chen C, Fang G (2010) *J Phys D Appl Phys* 43:145102
- Liu F, Zhang R, Hu Z, Sun J, Huang H, Li Z, Zhao J, Yin P, Guo L, Zhang X, Wang Y (2011) *IEEE Trans Plasma Sci* 39:700
- Liang M-H, Ho Y-T, Wang W-L, Peng C-Y, Chang L (2008) *J Cryst Growth* 310:1847
- Dai JN, Han XY, Wu ZH, Fang YY, Xiong H, Tian Y, Yu CH, He QH, Chen CQ (2011) *J Electron Mater* 40:446
- Jian S-R, Jang JS-C, Chen G-J, Chen H-G, Chen Y-T (2009) *J Alloys Compd* 479:348
- Dai JN, Han XY, Wu ZH, Yu CH, Xiang RF, He QH, Gao YH, Chen CQ, Xiao XH, Peng TC (2010) *J Alloys Compd* 489:519
- Chen JJ, Deng H, Li N, Tian YL, Ji H (2011) *Mater Lett* 65:716
- Chen JJ, Deng H, Ji H, Tian YL (2011) *Vac Sci Technol A* 29:03A116
- Pierce JM, Adekore BT, Davis RF, Stevie FA (2005) *J Cryst Growth* 283:147

46. Kashiwaba Y, Abe T, Nakagawa A, Endo H, Niikura I, Kashiwaba Y (2009) *Phys Status Solidi A* 206:944
47. Abe T, Kashiwaba Y, Onodera S, Masuoka F, Nakagawa A, Endo H, Niikura I, Kashiwaba Y (2007) *J Cryst Growth* 298:457
48. Tian J-S, Liang M-H, Ho Y-T, Liu Y-A, Chang L (2008) *J Cryst Growth* 310:777
49. Wang W-L, Peng C-Y, Ho Y-T, Chang L (2010) *Thin Solid Film* 518:2967
50. Ho Y-T, Wang W-L, Peng C-Y, Liang M-H, Tian J-S, Lin C-W, Chang L (2008) *Appl Phys Lett* 93:121911
51. Chou MM, Hang D-R, Wang SC, Chen C, Lee C-Y (2010) *J Cryst Growth* 312:1170
52. Chou MM, Hang D-R, Chen C, Wang SC, Lee C-Y (2011) *Mater Chem Phys* 125:791
53. Liang Y-C (2010) *J Alloys Comp* 508:158
54. Lin H, Zhou S, Zhou J, Liu X, Gu S, Zhu S, Xie Z, Han P, Zhang R (2008) *Thin Solid Film* 516:6079
55. Zhou S, Zhou J, Huang T, Li S, Zou J, Wang J, Zhang X, Li X, Zhang R (2007) *J Cryst Growth* 303:510
56. Zhang YW, Li XM, Yu WD, Yang C, Cao X, Gao XD, Kong JF, Shen WZ, Zhao JL, Sun XW (2009) *J Phys D Appl Phys* 42:075410
57. Lim S-H, Shindo D (2000) *J Appl Phys* 88:5107
58. Huang T, Zhou S, Teng H, Lin H, Wang J, Han P, Zhang R (2008) *J Cryst Growth* 310:3144
59. Yang AL, Song HP, Liang DC, Wei HY, Liu XL, Jin P, Qin XB, Yang SY, Zhu QS, Wang ZG (2010) *Appl Phys Lett* 96:151904
60. Zúñiga-Pérez J, Muñoz-Sanjosé V, Palacios-Lidón E, Colchero J (2006) *Appl Phys Lett* 88:261912
61. Kim J-H, Han SK, Hong SI, Hong S-K, Lee JW, Lee JY, Song J-H, Park JS, Yao T (2009) *J Vac Sci Technol B* 27:1625
62. Lee JW, Kim J-H, Han SK, Hong S-K, Lee JY, Hong SI, Yao T (2010) *J Cryst Growth* 312:238
63. Matsui H, Tabata H (2005) *Appl Phys Lett* 87:143109
64. Matsui H, Tabata H (2006) *J Appl Phys* 99:124307
65. Matsui H, Tabata H (2007) *Proc SPIE* 6474:647400
66. Matsui H, Tabata H (2010) *Proc SPIE* 7603:760307
67. Matsui H, Hasuike N, Harima H, Tabata H (2008) *J Appl Phys* 104:094309
68. Matsui H, Tabata H (2009) *Appl Phys Lett* 94:161907
69. Chou MM, Hang D-R, Chen C, Liao Y-H (2011) *Thin Solid Film* 519:3627
70. Yu J-Y, Huang T-H, Chang L, Liao Y-H, Chou M, Gan D (2011) *J Electrochem Soc* 158:H1166
71. Chou MM, Chang L, Chung H-Y, Huang T-H, Wu J-J, Chen C-W (2007) *J Cryst Growth* 308:412
72. Chou MM, Chang L, Hang D-R, Chen C, Chang D-S, Li C-A (2009) *Cryst Growth Des* 9:2073
73. Lin W-H, Wu J-J, Chou M, Chang L (2009) *Cryst Growth Des* 9:3301
74. Lin H, Zhou S, Teng H, Wang J (2009) *J Cryst Growth* 311:456
75. Lin H, Zhou S, Teng H, Hou X, Jia T, Gu S, Zhu S, Xie Z, Han P, Zhang R, Xu K (2009) *Appl Surf Sci* 255:9146
76. Cagin E, Yang J, Wang W, Phillips JD, Hong SK, Lee JW, Lee JY (2008) *Appl Phys Lett* 92:233505
77. Deng R, Yao B, Li YF, Li BH, Zhang ZZ, Zhao HF, Zhang JY, Zhao DX, Shen DZ, Fan XW, Yang LL, Zhao QX (2009) *J Cryst Growth* 311:4398
78. Ho Y-T, Wang W-L, Peng C-Y, Chen W-C, Liang M-H, Tian J-S, Chang L (2009) *Phys Status Solidi RRL* 3:109
79. Wang W-L, Ho Y-T, Chiu K-A, Peng C-Y, Chang L (2010) *J Cryst Growth* 312:1179
80. Wang W-L, Peng C-Y, Ho Y-T, Chuang S-C, Chang L (2011) *J Vac Sci Technol A* 29:031001
81. Diebold U, Koplitz LV, Dulub O (2004) *Appl Surf Sci* 237:336
82. Kroll M, Kuschel T, Löber T, Köhler U (2009) *Surf Sci* 603:L49
83. Sakaki H, Noda T, Hirakawa K, Tanaka M, Matsusue T (1987) *Appl Phys Lett* 51:1934
84. Zhou H, Chisholm MF, Pant P, Chang HJ, Gazquez J, Pennycook SJ, Narayan J (2010) *Appl Phys Lett* 97:121914
85. Ghosh S, Waltereit P, Brandt O, Grahm HT, Ploog KH (2002) *Phys Rev B* 65:075202
86. Zúñiga-Pérez J, Muñoz-Sanjosé V, Lorenz M, Benndorf G, Heitsch S, Spemann D, Grundmann M (2006) *J Appl Phys* 99:023514
87. Nam YS, Lee SW, Baek KS, Chang SK, Song J-H, Song J-H, Han SK, Hong S-K, Yao T (2008) *Appl Phys Lett* 92:201907
88. Tainoff D, Al-Khalifiou M, Deparis C, Vinter B, Teisseire M, Morhain C, Chauveau J-M (2011) *Appl Phys Lett* 98:131915
89. Akasaka S, Nakahara K, Tsukazaki A, Ohtomo A, Kawasaki M (2010) *Appl Phys Express* 3:071101
90. Ding P, Pan XH, Huang JY, He HP, Lu B, Zhang HH, Ye ZZ (2011) *J Cryst Growth* 331:15
91. Dai LP, Deng H, Chen JJ, Wei M (2007) *Solid State Commun* 143:378
92. Dai LP (2008) *Dissertation, University of Electronic Science and Technology of China*
93. Ko TS, Lu TC, Zhuo LF, Wang WL, Liang MH, Kuo HC, Wang SC, Chang Li, Lin DY (2010) *J Appl Phys* 108:073504
94. Chauveau J-M, Teisseire M, Kim-Chauveau H, Morhain C, Deparis C, Vinter B (2011) *J Appl Phys* 109:102420
95. Chauveau J-M, Teisseire M, Kim-Chauveau H, Deparis C, Morhain C, Vinter B (2010) *Appl Phys Lett* 97:081903
96. Chauveau J-M, Morhain C, Teisseire M, Laügt M, Deparis C, Zuniga-Perez J, Vinter B (2009) *Microelectron J* 40:512
97. Béaur L, Bretagnon T, Brimont C, Guillet T, Gil B, Tainoff D, Teisseire M, Chauveau J-M (2011) *Appl Phys Lett* 98:101913
98. Narayan J, Sharma AK, Kvit A, Jin C, Muth JF, Holland OW (2002) *Solid State Commun* 121:9